New *COL6A6* Variant Causes Autosomal Dominant Retinitis Pigmentosa in a Four-Generation Family

Veronika Vaclavik,[1,2] Leila Tiab,[3] Young Joo Sun,[4] Vinit B. Mahajan,[4,5] Alexandre Moulin,[1] Nathalie Allaman-Pillet,[3] Francis L. Munier,[1] and Daniel F. Schorderet[3,6,7]

[1]Jules-Gonin Eye Hospital, University of Lausanne, Lausanne, Switzerland
[2]Department of Ophthalmology, Hospital Cantonal, Fribourg, Switzerland
[3]Institute for Research in Ophthalmology, Sion, Switzerland
[4]Molecular Surgery Laboratory, Byers Eye Institute, Stanford University, Palo Alto, California, United States
[5]Veterans Affairs Palo Alto Health Care System, Palo Alto, California, United States
[6]Faculty of Life Sciences, Ecole Polytechnique Fédérale de Lausanne, Lausanne, Switzerland
[7]Faculty of Biology and Medicine, University of Lausanne, Lausanne, Switzerland

Correspondence: Veronika Vaclavik, Jules-Gonin Eye Hospital, University of Lausanne, Avenue de France 15, 1004 Lausanne, Switzerland; veronika.vaclavik@fa2.ch.

Received: June 22, 2021
Accepted: February 12, 2022
Published: March 25, 2022

Citation: Vaclavik V, Tiab L, Sun YJ, et al. New *COL6A6* variant causes autosomal dominant retinitis pigmentosa in a four-generation family. *Invest Ophthalmol Vis Sci.* 2022;63(3):23. https://doi.org/10.1167/iovs.63.3.23

Purpose. To report that variants in the gene for a large lamina basal component protein, *COL6A6* (collagen type VI alpha 6 chain, *Col6α6*), linked to chromosome 3p22.1 causes retinitis pigmentosa (RP) in patients with autosomal dominant transmission (adRP).

Methods. A positional-cloning approach, whole exome sequencing, and modeling were used. The proband and several affected family members have been phenotyped and followed for over 12 years.

Results. A heterozygous missense variant, c.509C>G (p. Ser170Cys) in exon 2 of *COL6A6* (comprised of 36 exons and 2236 amino acids), was observed in a four- generation family and is likely to cause the adRP phenotype. It was identified in 10 affected members. All affected family members had a distinct phenotype: late-onset rod cone dystrophy, with good retained visual acuity, until their late 70s. Immunohistochemistry of human retina showed a dot-like signal at the base of the inner segments of photoreceptors and outer plexiform layer (OPL). The structural modeling of the N7 domain of *Col6α6* suggests that the mutant might result in the abnormal cellular localization of collagen VI or malformation of collagen fibers resulting in the loss of its unique filament structure.

Conclusions. *COL6A6* is widely expressed in human tissues and evolutionary conserved. It is thought to interact with a range of extracellular matrix components. Our findings suggest that this form of RP has long-term useful central visual acuity and a mild progression, which are important considerations for patient counseling.

Keywords: *COL6A6*, collagen type VI alpha 6 chain, inherited retinal disease, retinitis pigmentosa, rod–cone dystrophy, genotype–phenotype correlation

Retinitis pigmentosa (RP) is a group of retinal diseases caused by primary or secondary death of photoreceptors and occurs in approximately 1 per 4000 individuals. Transmission may be autosomal or X-linked, dominant or recessive, and digenic inheritance or mitochondrial involvement has been reported in rare situations. Recent advances in technology, mainly the availability of whole exome sequencing (WES), have allowed the identification of a great number of genes. Those genes are mainly responsible for autosomal recessive forms of RP, as the mapping strategy is based on the identification of homozygous or compound heterozygous pathogenic or probable pathogenic variants. WES only rarely identifies allele dropouts (whole exon or gene deletions). Gain-of-function variants are also more complicated to evaluate and validate. In this report, we show that a dominant probable pathogenic variant in *COL6A6* results in autosomal dominant retinitis pigmentosa (adRP).

Materials and Methods

Clinical Sample Collection

The protocol of the study adhered to the tenets of the Declaration of Helsinki and was approved by the local ethics committee, Federal de la Sante Publique (DFSP 035.0003-48).

Subjects and Clinical Evaluation

The study was conducted in a four-generation Swiss/French family. Eighteen patients were affected with typical retinitis pigmentosa (Fig. 1). Some of them were admitted to the Jules-Gonin Eye Hospital in Lausanne and underwent a full ophthalmic and electrophysiological examination. Records sent by other treating ophthalmologists from France were reviewed when accessible. Subjects underwent color fundus

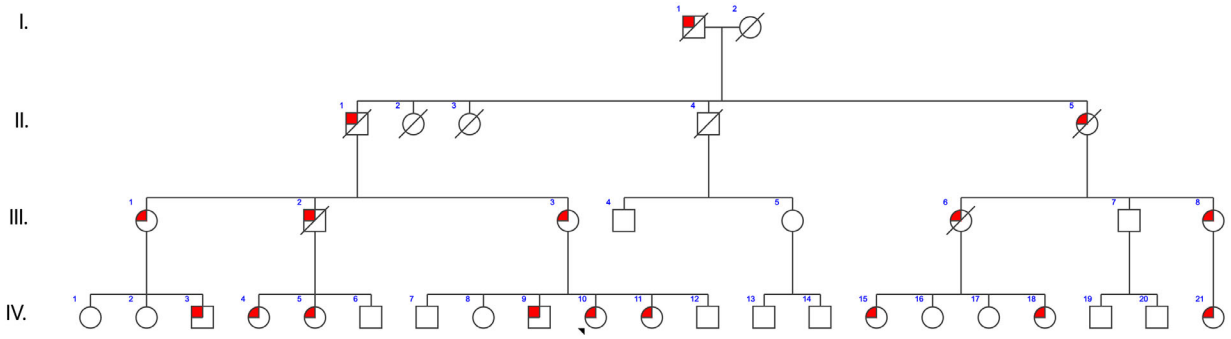

Figure 1. Pedigree structure of our Swiss/French family. The adRP-affected individuals are indicated by *red symbols*, and unaffected individuals are identified by *empty symbols*. The *black arrow* indicates the proband. The c.509C>G (p.Ser170Cys) variant in *COL6A6* segregated within all family members tested (patients III.1, III.2, III.3, III.6, III.8, IV.3, IV.9, IV.10, IV.15, and IV.21). Unaffected family members tested included IV.7, IV.8, and IV.12.

photography and autofluorescence (AF) imaging. AF imaging was obtained using a scanning laser ophthalmoscope (HRA2; Heidelberg Engineering, Heidelberg, Germany) by illuminating the fundus with argon laser light (488 nm) and viewing the resultant fluorescence through a bandpass filter with a short-wavelength cutoff at 495 nm. The proband also underwent widefield autofluorescence imaging with the use of Optomap (Optos, Dunfermline, UK).

Pupils were dilated using tropicamide 1% and phenylephrine hydrochloride 2.5% prior to electrophysiology testing. Full-field electroretinography (ERG) was performed using the International Society for Clinical Electrophysiology of Vision standards in the proband. The protocol included rod-specific and standard bright-flash ERG, both recorded after a minimum of 20 minutes of dark adaptation. Following 10 minutes of light adaptation, photopic 30-Hz flicker cone and transient cone ERGs were recorded. Further tests were performed including Goldman perimetry and optical coherence tomography (OCT) using the SPECTRALIS HRA2 (Heidelberg Engineering). Color testing was performed using Ishihara pseudoisochromatic plates.

Genetic Studies

After informed consent was obtained, blood samples from affected and unaffected family members were taken for DNA extraction. DNA was isolated from leucocytes (Nucleon BACC2; Amersham Biosciences, Amersham, UK). The transmission pattern of this four-generation family was consistent with autosomal dominant inheritance. A genome-wide linkage analysis was performed with 380 microsatellites from the ABI PRISM Linkage Mapping Set Version 2.5 (Thermo Fisher Scientific, Waltham, MA, USA), with an average distance between markers of 10 cm. Haplotypes were determined with an Autoscan V1.01B[1] and logarithm of the odds (LOD) scores were calculated using mLink 5.1[2] under the assumption of autosomal dominant inheritance with complete penetrance (new mutation rate of 0.001 and equal allele frequency). Two additional microsatellite markers, D3S1589 and D3S3606, in the vicinity of the rhodopsin gene (*RHO*) were used for linkage analysis.

Whole Exome Sequencing

WES was performed on the DNA of three affected individuals (III.1, III.6, and IV.10). The genotype was determined using the Affymetrix 250K single-nucleotide polymorphism (SNP) microarray platform (Thermo Fisher Scientific). WES of two of the patients was performed by Otogenetics Corporation (Atlanta, GA, USA) using the Roche NimbleGen 2 (44.1-megabase pair) paired-end sample preparation kit (Basel, Switzerland) and Illumina HiSeq 2500 System (Thermo Fisher Scientific) at a mean coverage of 30×. WES of the third patient was performed at CGC Genetics (Porto, Portugal). The quality control criteria for this analysis were total pass-filter (PF) reads, 125,171,510; unique PF reads, 115,774,525; percent Q score of 30 (Q30) bases, 91.49%; mean target coverage depth, 189.5; and percent autosome callability, 96.48%.

Bioinformatics Analysis

The obtained data were aligned using the human reference data hg19. Exome data were analyzed using the SNP & Variation Suite (Golden Helix, Bozeman, MT, USA) to identify variants that are shared between the affected individuals and then prioritized based on their absence/rarity in the general population, as reported in the publicly available databases dbSNP (http://www.ncbi.nlm.nih.gov/snp), 1000 Genomes (http://www.1000genomes.org), and gnomAD (https://gnomad.broadinstitute.org). The impact of missense variants on protein function was evaluated using Polymorphism Phenotyping v2 (PolyPhen-2),[3] PROVEAN,[4] and SIFT.[5] Only genes expressed in the eye with heterozygous variants were retained. We excluded synonymous variants and variants with a minor allele frequency higher than 0.01 as described in the 1000 Genomes or ExAC/gnomAD databases, as well as variants located in the non-coding sequence. Candidate variants were validated in affected individuals and in controls by conventional Sanger sequencing

Variant Analysis

Primers flanking the exons, introns, splice junction, and 5′ and 3′ untranslated regions (UTRs) were designed using Primer3 Input 0.4.0 for the candidate gene *RHO* evaluated by linkage analysis, and also primers flanking exon 2 of the candidate gene *COL6A6* (encoding collagen alpha-6(VI) chain [col6α6])[6] identified via exome sequencing. Each 20-µL PCR amplification reaction contained 10 µL of FastStart PCR Master Mix (Roche), 10 pmol of each primer (Eurogentec, Liège, Belgium), and 20 ng of genomic DNA. The

Investigative Ophthalmology & Visual Science

DNA was denatured at 95°C for 5 minutes prior to 35 cycles of amplification of 1 minute at 94°C, 1 minute at 58°C, 1 minute at 72°C, and a final extension step at 72°C for 10 minutes using a GeneAmp 9700 thermal cycler (Applied Biosystems, Waltham, MA, USA). The PCR products were resolved in 1% agarose gel stained with ethidium bromide. The amplified fragments were purified and sequenced in the forward direction using a BigDye Terminator Cycle Sequencing Kit (Applied Biosystems) and loaded onto an ABI Prism 3100 genetic analyzer (Applied Biosystems). The data were analyzed using ABI Prism Navigator software.

Immunohistochemistry

Sections (4 µm) were cut from paraffin-embedded, formalin-fixed tissues from eyes enucleated for uveal melanoma retrieved from the archives of the pathology laboratory at Jules-Gonin Eye Hospital (local ethics committee authorization 340/15). After blocking endogenous peroxidase by 4% hydrogen peroxide for 10 minutes and antigenic unmasking at pH 6, the sections were incubated for 60 minutes with anti-*COL6A6* antibody (HPA045239, 1/1000 dilution; Atlas Antibodies, Stockholm, Sweden). A streptavidin/biotin detection method with 3,3′-diaminobenzidine tetrachloride was used for signal detection (Dako EnVision+ Dual-Link System–HRP; Agilent Technologies, Santa Clara, CA, USA).

Structural Modeling of N7 Domain of col6α6

The online PHYRE2 server[7] was used to generate the homology-based structural model of col6α6 N7 domain. The model (residues 25–217) was generated with high confidence based on the p.Arg1061Gln mutant structure of col6α3 (PDB ID, 4IHK). The figure was generated using Pymol.[8]

Results

The index individual in family 1 (IV.10) was a 67-year-old female who had suffered from night blindness since she was 15 years old. When she first came to the Jules-Gonin Eye Hospital, visual acuity (VA) was 20/20 in both eyes, corrected with −3.50 D = −3.25/2° in the right eye and −1.5D = −2.75/163° in the left eye. Seven years later, her VA declined to 20/35 partly due to bilateral early lens sclerosis. Fundus examination showed some bone spicules at the mid-periphery with no macula abnormalities (Figs. 2A, 2B). Rod-specific ERGs were undetectable, whereas photopic ERGs were severely reduced. Peripheral visual field constriction via an I-4e isopter, as measured by Goldman kinetic perimetry, was within 10°, whereas it was 75° horizontally with a V-4e isopter. There was a relative scotoma at the mid-periphery. OCT did not show any macular edema. The outer nuclear layer, ellipsoid zone, and external limiting membrane (ELM) were well preserved at the level of the fovea and then disappeared outside fovea (Figs. 2E, 2F). Autofluorescence imaging showed a decrease or lack of autofluorescence around the optic nerve and alongside retinal temporal arcades (Figs. 2C, 2D, 3A, 3B). Over the 12-year follow-up, the AF images showed an increase of hypofluorescent areas near the optic nerve and along and beyond the arcades. Over the same period, there was mild constriction of the hyperautofluorescent ring (Figs. 3C, 3D). The proband's affected brother (IV.9) also suffered from night blindness, since his early 20s. When he was 26 years old, he tried to become a train driver but never received authorization due to visual field constriction. Currently 68 years of age, he has a best-corrected visual acuity of 10/20 in the right eye and 15/20 in the left eye. He had bilateral macular edema, which improved following treatment (anti-vascular endothelial growth factor or dexamethasone implant intravitreal injections). Both patients were from a non-consanguineous family originating from Switzerland, with 18 affected individuals. The age of onset of symptoms within family members started in their mid-teens and early 20s, with night blindness and peripheral visual field constriction. The mother of the proband (III.3) lost her central vision when she was 80 years old. Her father (II.1) was blind when he died at the age of 75 years. One unaffected brother of the proband (IV.7) had been assessed by a private ophthalmologist in France when he was 58 years old. He underwent a complete ophthalmological and fundus examination and visual field evaluation, with results within normal limits. Currently 71 years old, he is still driving. No family member reported having a myopathy, atopic dermatitis, or any other major health condition.

Combined Genetic Mapping and Whole Exome Sequencing

In this family, we performed genome-wide linkage analysis and found a maximum LOD score of 1.51 at marker D3S3606. Ten of the affected patients who agreed to genetic testing were studied (Fig. 1; patients III.1, III.2, III.3, III.6, III.8, IV.3, IV.9, IV.10, IV.15, and IV.21). Haplotype analysis showed that affected individuals in the family shared a common haplotype delimited by markers D3S1589 and D3S1292, a region of approximately 5.7 Mb at 3q21 (Fig. 1). As this interval contained the *RHO* gene, all of its five exons, complete introns, 5′-UTR (600 bp upstream of the start codon ATG), and 3′-UTR (600 bp downstream of the stop codon TAA) were directly sequenced in two affected individuals, and none of them had variation in this gene. Multiplex ligation-dependent probe amplification analysis did not show any deletion of duplication. We used a combination of linkage studies and WES to elucidate the disease-causing variant. WES was performed in three affected individuals (Fig. 1; patients III.1, III.8, and IV.10).

Comparison of the whole exome data for the first two patients identified 484 genes expressed in the eye and non-synonymous variants that were novel or rare (<1%). Three genes located within or close to the linked region (*PLXNA1*, *COL6A6*, and *TOPBP1*) showed heterozygous variants and were tested for variant co-segregation in the family. None of the variants present in the selected genes segregated in affected individuals except for the heterozygous missense variant c.509C>G (p.Ser170Cys) in exon 2 of *COL6A6* (ENST00000358511.10) which was present in all 10 affected members. WES of the third patient confirmed the absence of pathogenic or probable pathogenic variant in *RHO*. This variant is novel and is predicted to be damaging by the PolyPhen-2 tool, with a score of 0.999; deleterious by PROVEAN, with a score of −3.370; and influencing protein function by SIFT, with a score of 0.01. This new variant was absent from non-affected family members tested (Fig. 1; patients IV.7, IV.8, and IV.12) and had not been described in gnomAD as of November 27, 2021.

Immunofluorescence Analysis

Type VI collagen is a subgroup of unconventional and network-forming collagens. It is ubiquitously expressed in

Investigative Ophthalmology & Visual Science

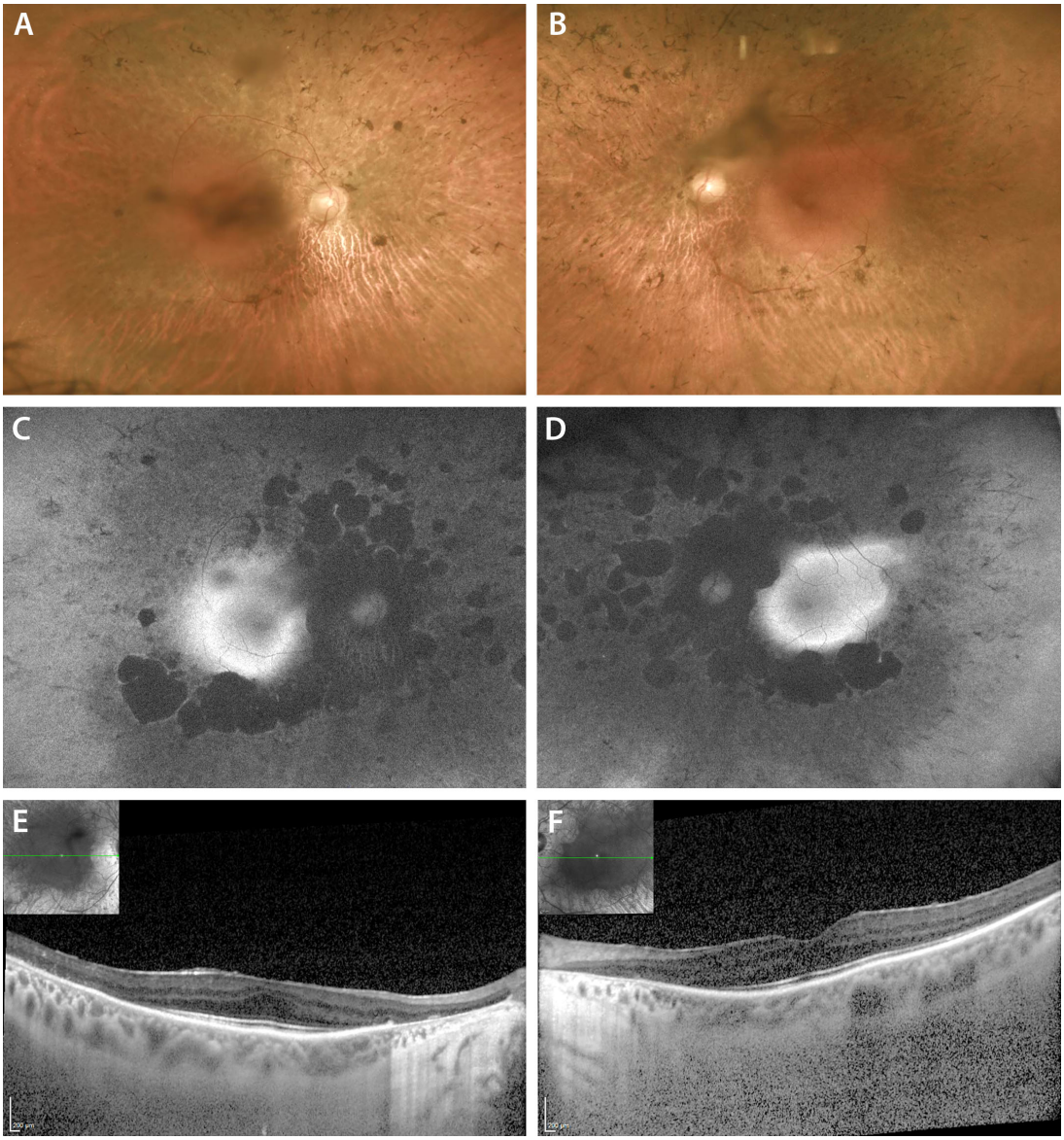

Figure 2. Fundus color, AF, and OCT of both eyes of the proband. (**A**, **B**) Fundus color showing bone spikes and signs of retinal atrophy nasal to the optic nerve and alongside arcades. (**C**, **D**) Hypoautofluorescence around the optic nerve, alongside arcades and patches of hypofluorescence nasal to the optic nerve. (**E**, **F**) OCT did not show any macular edema. The outer nuclear layer, ellipsoid zone, and ELM are well preserved at the level of the fovea and then disappear outside the fovea.

humans and plays important roles in tissue repair,[9] neuron protection, injury response,[10] and corneal development.[11–13] Pathogenic or probable pathogenic variants in collagen VI compartments are reported to cause myopathies, including Bethlem myopathy. We assessed the expression of col6α6 by immunohistochemistry in healthy human retinas from enucleated eyes. Although there was a diffuse staining in the retina including some nuclei, a dot-like signal could clearly be identified at the base of the inner segments of photoreceptors and in the outer plexiform layer (Fig. 4A).

Collagen VI has a unique molecular structure that forms beaded filaments.[14] The generally understood chain composition of collagen VI is α1(VI)α2(VI)α3(VI) heterotrimer helix; yet, the α3(VI) can potentially be substituted by α6(VI) coded by the *COL6A6* gene.[15,16] The α6(VI) consists of seven N-terminal von Willebrand factor A (VWA) domains (also referred to as N7–N1 domains) followed by a collagenous domain, two C-terminal VWA domains (also referred to as C1 and C2 domains), and a unique domain also known as C3 domain (Fig. 5A).[17] The interaction among the collagenous domains of α1(VI), α2(VI), and α6(VI) drives the heterotrimer helix chain formation of collagen VI (Fig. 5B), which is necessary for secretion of the chain.[18] When the chains are made, they assemble into a dimer and then form tetramers (Fig. 5C). Upon secretion and deposition of these tetramers in the extracellular matrix, the non-collagenous domains (i.e., N7–N1 and C1–C3 domains) contribute to the formation of beaded filaments (supramolecular aggregations) through metal ion–dependent adhesion and/or conserved hydrophobic moieties (Fig. 5D).[15,19–21]

The heterozygous missense variant (c.509 C>G; p.Ser170Cys) in *COL6A6* is located in the N7 domain. Structural modeling of the mutant col6α6 N7 domain demonstrates that the variant is located at the β4–α5 loop

Investigative Ophthalmology & Visual Science

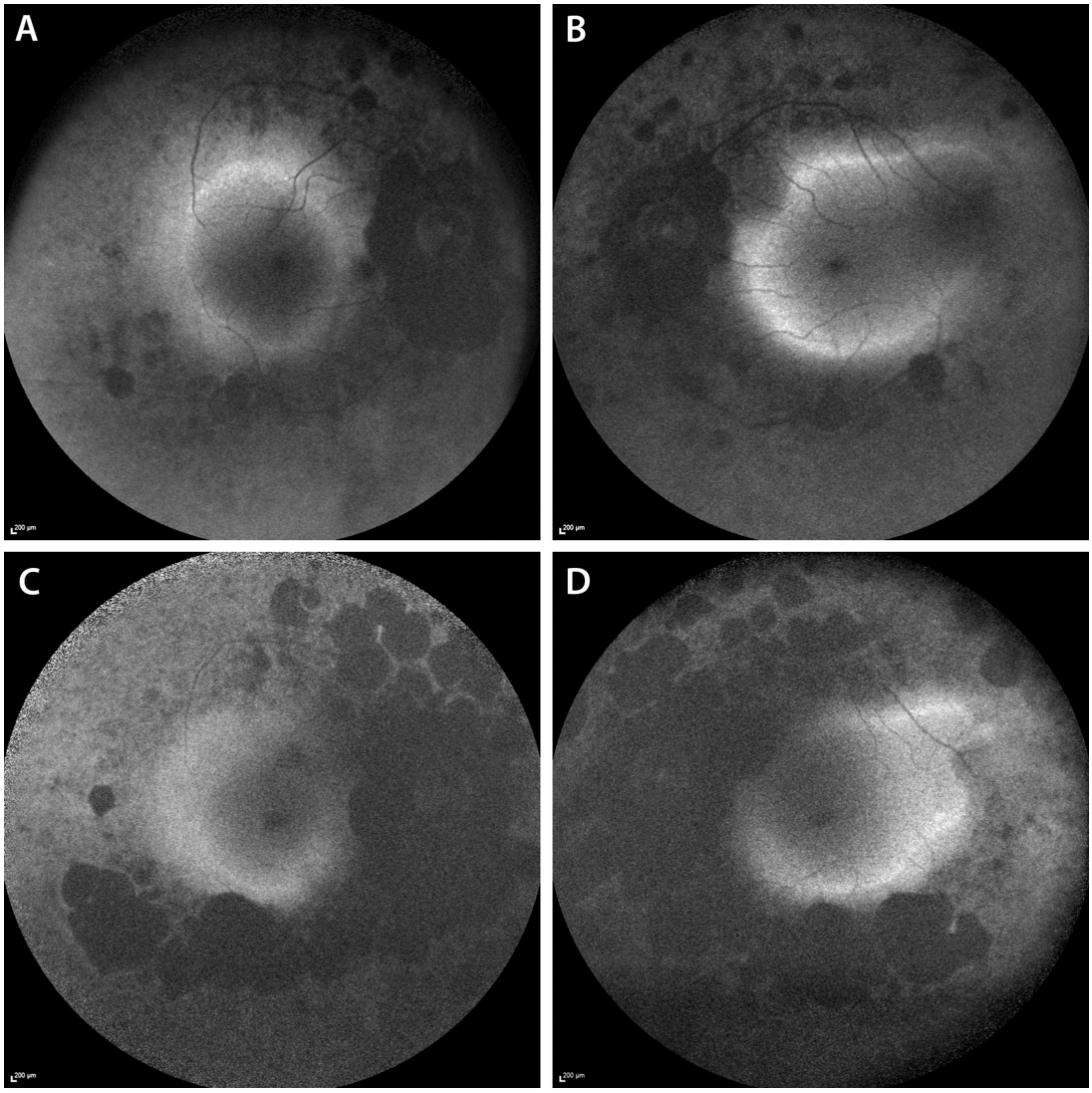

Figure 3. AF imaging over 12 years of follow-up. (**A**, **B**) There is a decrease of AF around the optic nerve and alongside retinal temporal arcades. (**C**, **D**) Over the years, the AF images showed an increase of hypofluorescent areas around the optic nerves, along and beyond the arcades. Over the same period, there was a very mild constriction of the hyperautofluorescent ring.

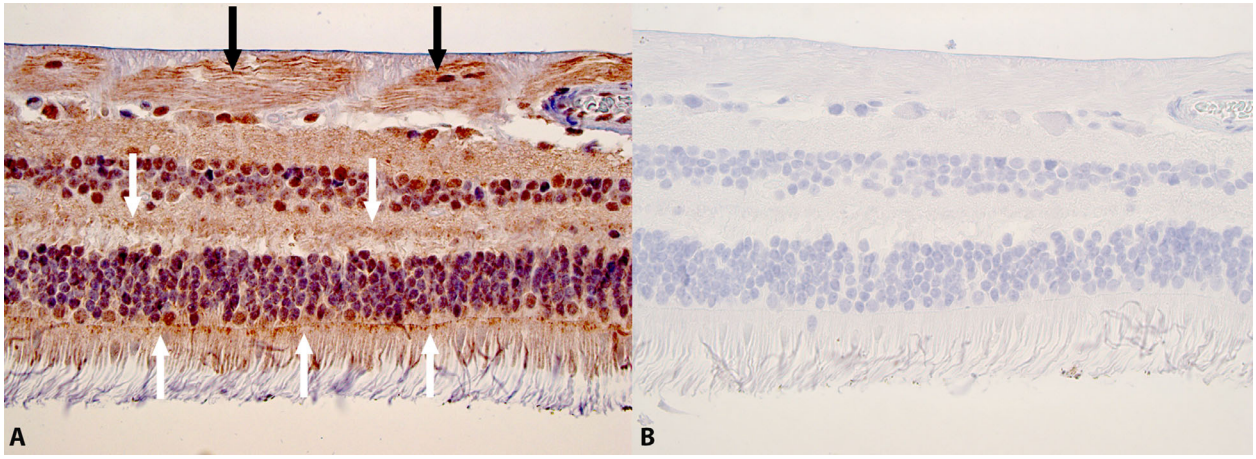

Figure 4. Immunohistochemistry of *COL6A6* expression in human retina. (**A**) *COL6A6* expression could be diffusely identified in the retina with marked expression in the nerve fiber layers (*black arrows*) and a dot-like expression in the outer plexiform layer (*downward white arrows*), as well as in the inner segments of photoreceptors close to the ELM (*upward white arrows*). (**B**) Matched negative retinal control (magnification 252×).

Investigative Ophthalmology & Visual Science

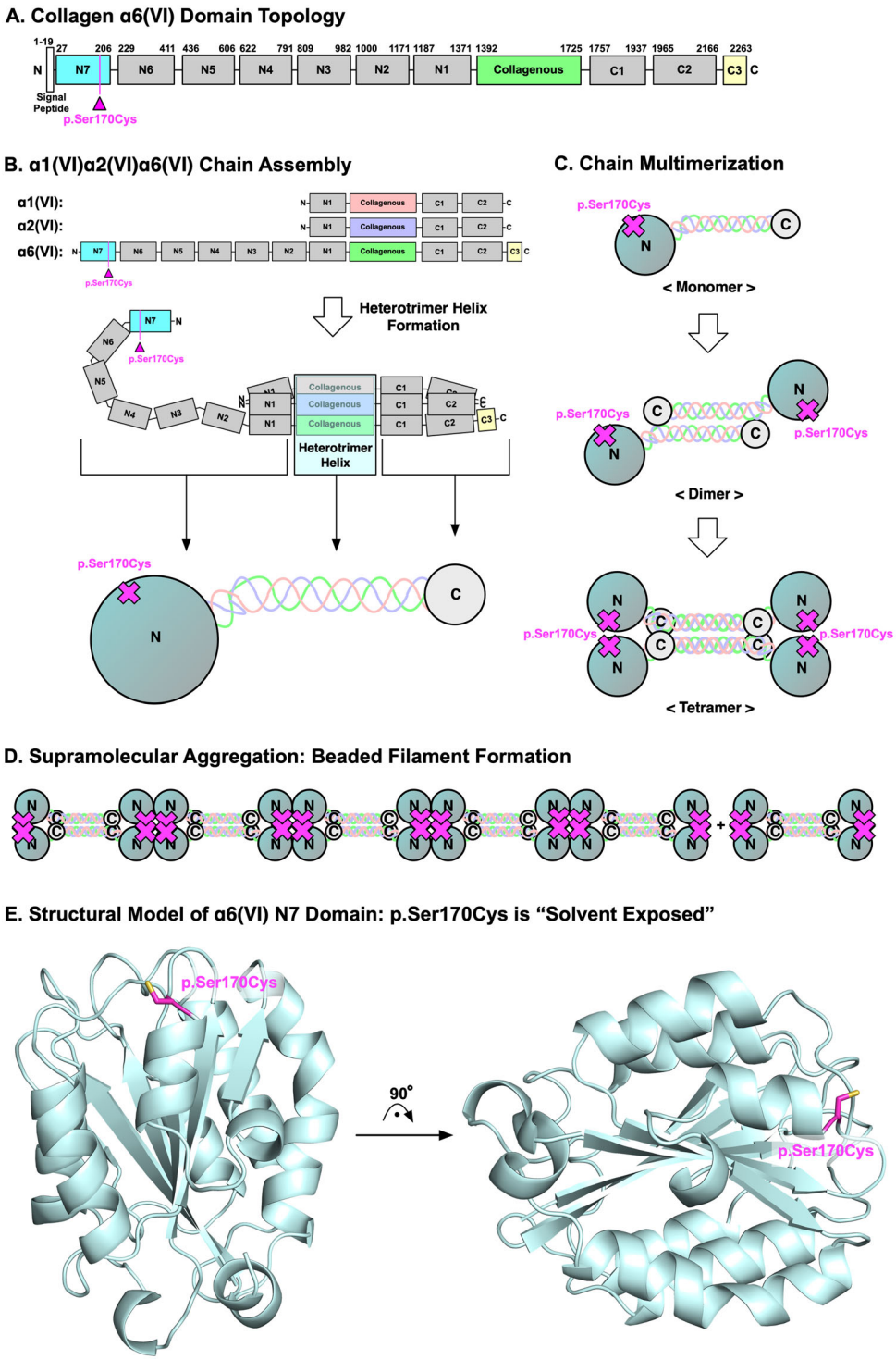

Figure 5. Collagen α6(VI) domain topology and structural modeling highlight the potential defects of the patient mutant in the collagen-formation dynamics. The patient variant (p.Ser170Cys) is highlighted in *magenta* throughout the figure. (**A**) Domain topology of collagen α6(VI). The N7 domain (the first VWA domain) that includes our patient variant is shown in the *cyan box*. Other VWA domains (N6–N1 and C1–C2) are shown in the gray boxes. The collagenous domain is shown in the *green box*. The unique domain (C3) is shown in the *yellow box*. (**B**) Illustration of the α1(VI)α2(VI)α6(VI) chain assembly in an intracellular space. The collagenous domains from each collagen VI protein form a heterotrimer helix resulting in a chain monomer. The clusters of N domains are represented as a *cyan–gray circle*, and the C domain cluster is represented by the *gray circle*. (**C**) Representation of the collagen VI chain multimerization in an intracellular space. Two monomer chains form a dimer, then two dimers form a tetramer. After tetramer formation, it will be secreted to an extracellular space. (**D**) Representation of collagen VI filament formation at an extracellular region. The non-collagenous domains at the end of each tetramer join to form a bead-like structure resulting in a beaded filament. (**E**) The homology-based structural model of the collagen α6(VI) p.Ser170Cys mutant N7 domain. It was modeled from the VWA structure of collagen α3(VI) (PDB ID, 4IHK). The mutant cysteine was exposed to solvent. This suggests that the mutant cysteine may be freely available to form disulfide bonds with the cysteines of itself, other collagen building blocks, or non-specific proteins. This might significantly affect the dynamics of collagen filament formation and result in abnormal collagen VI filament structures.

Investigative Ophthalmology & Visual Science

of the domain and is solvent exposed (Fig. 5E). The serine-to-cysteine change at the loop region is unlikely to disrupt protein stability, but the surface-exposed cysteine can form nonspecific disulfide interactions with freely available cysteines in other proteins. Thus, this additional cysteine in the mutant may significantly disrupt chain assembly dynamics and/or the supramolecular aggregation dynamics of collagen VI. These may result in the abnormal cellular localization of collagen VI compartments or malformation of collagen fibers, resulting in the loss of its unique beaded filament structure. Additionally, it may affect the accessibility of the collagen-binding proteins and lead to abnormal cellular signaling events.

Discussion

In this report, we describe a four-generation family with adRP, likely due to a c.509C>G (p.Ser170Cys) heterozygous missense variant in *COL6A6* that segregated in all affected members. Our family has a very mild rod–cone retinal dystrophy, with slow progression, and they have retained central VA until their mid-70s, with the eldest members losing his VA in his late 70s. In a previous report,[22] a *COL6A6* variant was also detected in an adRP pedigree; however, that variant was linked to deletion of exon 5 in *RHO*, the *COL6A6* variant, and deletion segregating in all affected members. That family also showed mild progression of rod–cone dystrophy.

COL6A6 (OMIM 131873) is located on chromosome 3q22.1 and contains 36 exons. It encodes a large protein that is a component of the basal lamina of epithelial cells. In human normal tissue, *COL6A6* is mainly expressed in lung, fat, heart, spleen, and skeletal and cardiac muscle.[23] Its expression in the retina has been reported by de Sousa Dias et al.,[22] who used PCR amplification of a fragment from retinal cDNA containing juxtaposing sequences of exons 2 and 3.

Our results demonstrated a dot-like expression of *COL6A6* in the inner segments of the photoreceptors and in the outer plexiform layer, as well as a diffuse staining in the retina. These findings are in line with single-cell RNA expression from the human protein atlas where *COL6A6* has been mainly identified in rod photoreceptors and bipolar cells (https://www.proteinatlas.org/ENSG00000206384-COL6A6/celltype/eye). *COL6A6* has been identified only recently, together with *COL6A4* and *COL6A5*,[24] at the same 3p22.1 locus and is evolutionarily conserved. It encodes the α6(VI) chain, containing a 336-amino acid triple helix flanked by seven N-terminal VWA-like domains. Collagen VI interacts with a range of extracellular matrix components. Due to its wide expression, *COL6A6* is suspected to be involved in early-onset atopic dermatitis,[25] as well as collagen VI–related myopathies.[26] *COL6A6* is also suspected of playing a causative role in ossification of the posterior longitudinal ligament of the thoracic spine in Chinese populations.[27]

Other collagen genes have been widely described as being causative of syndromic RP. *COL2A1* is well known in Stickler syndrome (SS; MIM 108300),[28] a progressive hereditary arthro-ophthalmopathy of collagen connective tissue with an associated RP phenotype recently reported.[29] Retinal perivascular hyperpigmentation[30] and retinal perivascular degeneration have also been described as a consistent finding in patients with SS and variants in the *COL2A1* gene.[31]

Variants in others collagen genes have been reported to cause several subtypes of SS (*COL9A1*, *COL9A2*, and *COL9A3*) with variable retinal phenotypes, ranging from progressive chorioretinal degeneration, lattice degeneration, and retinal detachment to normal.[32] More studies are needed to confirm these preliminary findings. This will enable a better understanding of the function of *COL6A6*, which may be deemed to be part of the panel of adRP genes.

Acknowledgments

The authors would like to thank the family, mainly the proband, for her impressive and dedicated help.

Disclosure: **V. Vaclavik,** None; **L. Tiab,** None; **Y.J. Sun,** None; **V.B. Mahajan,** None; **A. Moulin,** None; **N. Allaman-Pillet,** None; **F.L. Munier,** None; **D.F. Schorderet,** None

References

1. Hiekkalinna T, Peltonen L. New program: AUTOSCAN 1.0 automated use of linkage analysis programs. *Am J Human Genet*. 1999;65:A254–A254.
2. Lathrop GM, Lalouel JM, Julier C, Ott J. Strategies for multilocus linkage analysis in humans. *Proc Natl Acad Sci USA*. 1984;81:3443–3446.
3. Adzhubei I, Jordan DM, Sunyaev SR. Predicting functional effect of human missense mutations using PolyPhen-2. *Curr Protoc Hum Genet*. 2013;Ch7:Unit7.20.
4. Choi Y, Chan AP. PROVEAN web server: a tool to predict the functional effect of amino acid substitutions and indels. *Bioinformatics*. 2015;31:2745–2747.
5. Sim NL, Kumar P, Hu J, Henikoff S, Schneider G, Ng PC. SIFT web server: predicting effects of amino acid substitutions on proteins. *Nucleic Acids Res*. 2012;40:W452–W457.
6. Tagliavini F, Pellegrini C, Sardone F, et al. Defective collagen VI α6 chain expression in the skeletal muscle of patients with collagen VI-related myopathies. *Biochim Biophys Acta*. 2014;1842:1604–1612.
7. Kelley LA, Mezulis S, Yates CM, Wass MN, Sternberg MJ. The Phyre2 web portal for protein modeling, prediction and analysis. *Nat Protoc*. 2015;10:845–858.
8. Schrödinger L. The PyMOL Molecular Graphics System, Version 2.0 Schrödinger, LLC. Available at: https://pymol.org/2/support.html? Accessed February 24, 2022.
9. Schnoor M, Cullen P, Lorkowski J, et al. Production of type VI collagen by human macrophages: a new dimension in macrophage functional heterogeneity. *J Immunol*. 2008;180:5707–5719.
10. Cheng L-C, Pastrana E, Tavazoie M, Doetsch F. miR-124 regulates adult neurogenesis in the subventricular zone stem cell niche. *Nat Neurosci*. 2009;12:399.
11. Doane KJ, Howell SJ, Birk DE. Identification and functional characterization of two type VI collagen receptors, alpha 3 beta 1 integrin and NG2, during avian corneal stromal development. *Invest Ophthalmol Vis Sci*. 1998;39:263–275.
12. Doane KJ, Yang G, Birk DE. Corneal cell-matrix interactions: type VI collagen promotes adhesion and spreading of corneal fibroblasts. *Exp Cell Res*. 1992;200:490–499.
13. Takahashi T, Cho HI, Kublin CL, Cintron C. Keratan sulfate and dermatan sulfate proteoglycans associate with type VI collagen in fetal rabbit cornea. *J Histochem Cytochem*. 1993;41:1447–1457.
14. Gordon MK, Hahn RA.Collagens. *Cell Tissue Res*. 2010;339:247–257.

15. Gara SK, Grumati P, Urciuolo A, et al. Three novel collagen VI chains with high homology to the alpha3 chain. *J Biol Chem*. 2008;283:10658–10670.
16. Bächinger HP, Mizuno K, Vranka JA, Boudko SP. Collagen formation and structure. In: Liu H-W, Mander L , eds. *Comprehensive Natural Products II: Chemistry and Biology*. Amsterdam: Elsevier; 2010:469–530.
17. Ricard-Blum S. The collagen family. *Cold Spring Harb Perspect Biol*. 2011;3:a004978.
18. Bonaldo P, Braghetta P, Zanetti M, Piccolo S, Volpin D, Bressan GM. Collagen VI deficiency induces early onset myopathy in the mouse: an animal model for Bethlem myopathy. *Hum Mol Genet*. 1998;7:2135–2140.
19. Lee J-O, Rieu P, Arnaout MA, Liddington R. Crystal structure of the A domain from the a subunit of integrin CR3 (CD11b/CD18). *Cell*. 1995;80:631–638.
20. Perkins SJ, Smith KF, Williams SC, Haris PI, Chapman D, Sim RB. The secondary structure of the von Willebrand factor type A domain in factor B of human complement by Fourier transform infrared spectroscopy: its occurrence in collagen types VI, VII, XII and XIV, the integrins and other proteins by averaged structure predictions. *J Mol Biol*. 1994;238:104–119.
21. Furthmayr H, Wiedemann H, Timpl R, Odermatt E, Engel J. Electron-microscopical approach to a structural model of intima collagen. *Biochem J*. 1983;211:303–311.
22. de Sousa Dias M, Hernan I, Delás B, et al. New *COL6A6* variant detected by whole-exome sequencing is linked to break points in intron 4 and 3′-UTR, deleting exon 5 of RHO, and causing adRP. *Mol Vis*. 2015;21:857–870.
23. Fagerberg L, Hallström BM, Oksvold P, et al. Analysis of the human tissue-specific expression by genome-wide integration of transcriptomics and antibodybased proteomics. *Mol Cell Proteomics*. 2014;13:397–406.
24. Fitzgerald J, Rich C, Zhou FH, Hansen U. Three novel collagen VI chains, α4 (VI), α5 (VI), and α6 (VI). *J Biol Chem*. 2008;283:20170–20180.
25. Heo WI, Park KY, Jin T, et al. Identification of novel candidate variants including *COL6A6* polymorphisms in early-onset atopic dermatitis using whole-exome sequencing. *BMC Med Genet*. 2017;18:8.
26. Tagliavini F, Pellegrini C, Sardone F, et al. Defective collagen VI α6 chain expression in the skeletal muscle of patients with collagen VI-related myopathies. *Biochim Biophys Acta*. 2014;1842:1604–1612.
27. Liang C, Wang P, Liu X, et al. Whole-genome sequencing reveals novel genes in ossification of the posterior longitudinal ligament of the thoracic spine in the Chinese population. *J Orthop Surg Res*. 2018;13:324.
28. Stickler GB, Belau PG, Farrell FJ, et al. Hereditary progressive arthro-ophthalmopathy. *Mayo Clin Proc*. 1965;40:433–455.
29. Breazzano MP, Coleman DJ, Chen RW, Chang S, Daly S, Tsang SH. Prospective impact of sildenafil on chronic central serous chorioretinopathy. *Ophthalmol Retina*. 2020;4:1119–1123.
30. Breazzano MP, Tsang SH, Tezel TH. Stickler syndrome genotype (COL2A1 mutation) with retinitis pigmentosa phenotype. *Ophthalmol Retina*. 2020;4:522.
31. Parma ES, Körkkö J, Hagler WS, Ala-Kokko L. Radial perivascular retinal degeneration: a key to the clinical diagnosis of an ocular variant of Stickler syndrome with minimal or no systemic manifestations. *Am J Ophthalmol*. 2002;134:728–734.
32. Nixon TR, Alexander P, Richards A, et al. Homozygous type IX collagen variants (COL9A1, COL9A2, and COL9A3) causing recessive Stickler syndrome-expanding the phenotype. *Am J Med Genet A*. 2019;179:1498–1506.